Journal of Power Sources 332 (2016) 230–239

Contents lists available at ScienceDirect

Journal of Power Sources

journal homepage: www.elsevier.com/locate/jpowsour

Suppressing capacity fading and voltage decay of Li-rich layered cathode material by a surface nano-protective layer of CoF_2 for lithium-ion batteries

Shaokun Chong [a], Yuanzhen Chen [a], Wuwei Yan [a], Shengwu Guo [a], Qiang Tan [a], Yifang Wu [b], Tao Jiang [a], Yongning Liu [a, *]

[a] State Key Laboratory for Mechanical Behavior of Materials, School of Material Science and Engineering, Xi'an Jiaotong University, Xi'an, 710049, PR China
[b] Northwest Institute for Nonferrous Metal Research, Xi'an, 710016, PR China

HIGHLIGHTS

- Nano-CoF_2 is firstly coated on $Li_{1.2}Ni_{0.2}Mn_{0.6}O_2$ via a wet chemistry method.
- 0.5% CoF_2-coated sample delivers the improved initial coulombic efficiency of 86.2%.
- Excellent stability of capacity and voltage are observed for 1.0% CoF_2-coating.
- The mechanisms of serious fading of capacity and voltage are discussed in details.
- Structure transition is suppressed by CoF_2 nano-coating evidenced by TEM analysis.

GRAPHICAL ABSTRACT

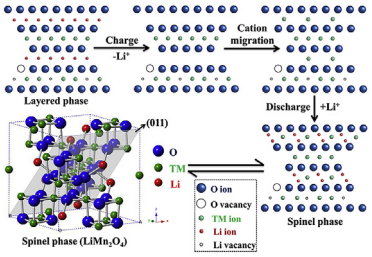

ARTICLE INFO

Article history:
Received 8 July 2016
Received in revised form
2 September 2016
Accepted 6 September 2016
Available online 29 September 2016

Keywords:
Lithium-ion battery
Cathode material
CoF_2 coating layer
Capacity fading
Voltage decay

ABSTRACT

Li-rich layered oxides have been regarded as valuable cathode materials for high energy density lithium-ion batteries. However, high initial irreversible capacity, bad rate capability, as well as serious capacity fading and voltage decay hinder their commercial application. In this paper, a nano CoF_2 protective layer is coated on the surface of $Li_{1.2}Ni_{0.2}Mn_{0.6}O_2$ via a facial wet chemistry method. A high initial discharge capacity of 264.4 mAh g^{-1} is obtained for 0.5% CoF_2-coated sample and 259.1 mAh g^{-1} for 1% CoF_2-coated sample owing to the suppression of irreversible release of O_2 and the contribution of electrochemical conversion of CoF_2/LiF. Furthermore, 1% CoF_2-coated sample exhibits the excellent rate capability of 167.5 mAh g^{-1} at 5 C rate, the superior cycling stability with the capacity retention of 241.0 mAh g^{-1} and the ameliorative voltage drop of 0.312 V at 0.1C after 100 cycles. The enhanced rate performance as well as stability of capacity and voltage can be attributed to the nano coatings which inhibit the electrolyte-electrode side reaction, enhance the electrochemical kinetics and mitigate structure transition from layered to spinel phase.

© 2016 Elsevier B.V. All rights reserved.

1. Introduction

To meet more demanding requirements for portable electronics, electric vehicles and hybrid electric vehicles, rechargeable lithium-

* Corresponding author.
E-mail address: ynliu@mail.xjtu.edu.cn (Y. Liu).

http://dx.doi.org/10.1016/j.jpowsour.2016.09.028
0378-7753/© 2016 Elsevier B.V. All rights reserved.

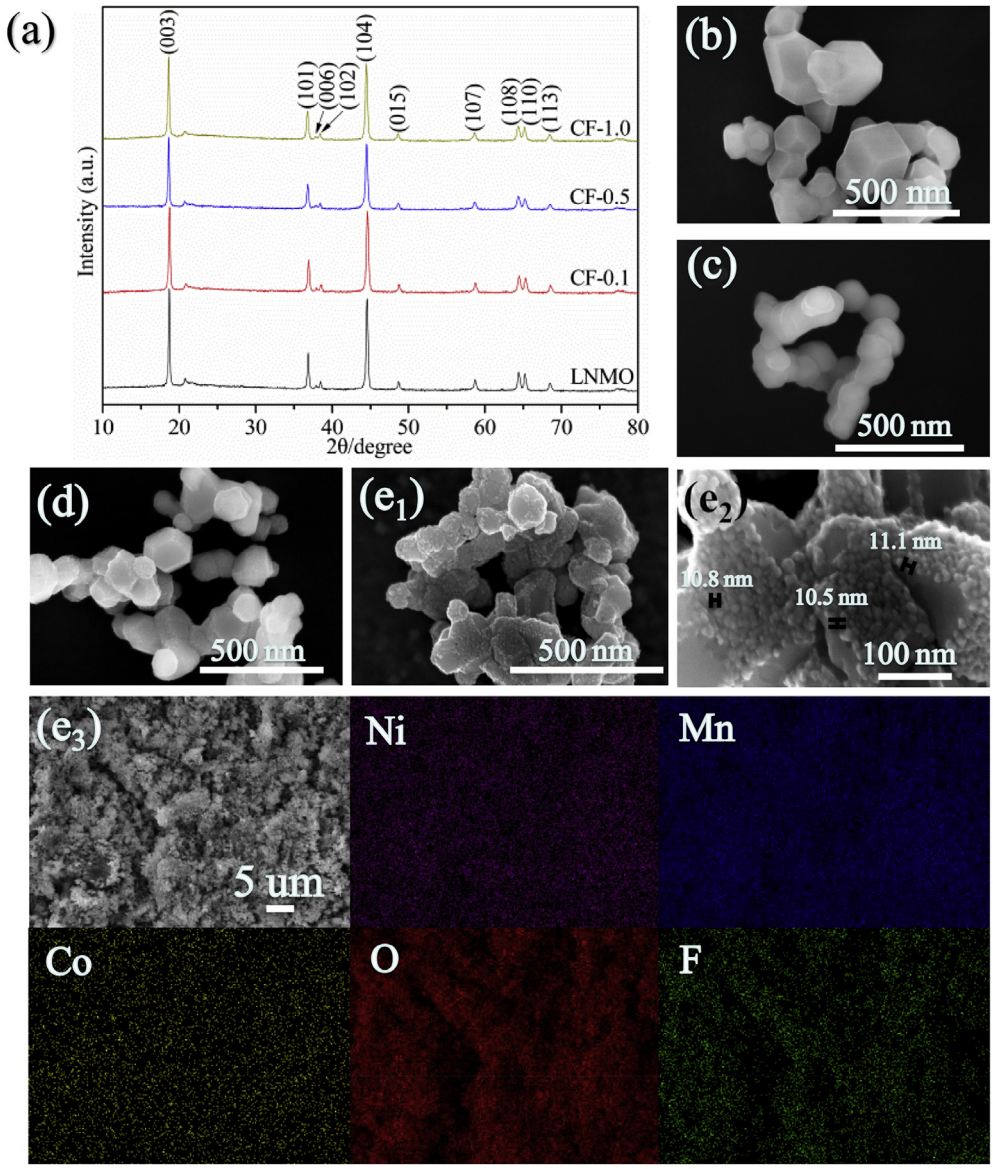

Fig. 2. (a) XRD patterns of pristine LNMO, CF-0.1, CF-0.5 and CF-1.0; SEM images of (b) LNMO, (c) CF-0.1, (d) CF-0.5 and (e_1) CF-1.0; (e_2 and e_3) high magnification SEM image and EDS elemental mapping of CF-1.0.

Table 1
The lattice parameters and the ratios of *c/a* for samples calculated from the XRD data.

Sample	*a*/Å	*c*/Å	*c/a*
LNMO	2.8661	14.2504	4.972
CF-0.1	2.8552	14.2306	4.950
CF-0.5	2.8585	14.2476	4.981
CF-1.0	2.8603	14.2558	4.989

is more, the interplanar spacing of the lattice fringes at the edge region is measured to be 2.86 Å, indexed to the (111) plane of cubic CoF_2 (Fig. 3(g)), which demonstrates that nano-layer of CoF_2 has been successfully coated on the surface of LNMO.

The EDS analysis of CF-1.0 sample measured by TEM was performed to verify the chemical composition of coating layer. The EDS elemental mapping clearly reveals that the Co and F elements are uniformly distributed on the surface of LNMO particle in Fig. 3(h), and it is clearly found that the edge of particle exists more Co and F elements compared to Ni, Mn and O elements, indicating that the coating layer is composed of Co and F ions. The EDS line scan provides that the intensities of Ni, Mn and O elements decrease gradually from the inner to edge, while Co and F elements present opposite tendency that the intensities increase from the inner to edge in Fig. 3(i), further providing an evidence to prove the results of TEM analysis.

With the purpose of further confirming the existence of CoF_2 coating layer on the surface of LNMO, XPS was carried out, as shown in Fig. 4. As for all the samples, the binding energies (BEs) of $Ni_{2p3/2}$ (Fig. 4(a)) and $Mn_{2p3/2}$ (Fig. 4(b)) are located at 854.7 eV and 642.4 eV, respectively, in good agreement with the values of Ni^{2+} and Mn^{4+} in layered oxides $Li[Li_{1/3-2x/3}Ni_xMn_{2/3-x/3}]O_2$ [38,39]. In addition, the $Co_{2p3/2}$ peaks of CoF_2-coated samples at 781.8 eV in Fig. 5(c) can be assigned to the Co—F bond [40], and the BEs of F_{1s} peaks are observed at 687.0 eV in Fig. 5(d) corresponding to the F-M bonding [41]. Also, the intensities of Ni_{2p} and Mn_{2p} decrease as the coating layer increases, while the intensities of Co_{2p} and F_{1s} increase with the content of CoF_2 within the XPS probing depth. All the XPS data further indicate that CoF_2 phase was coated on the surface of bare LNMO.

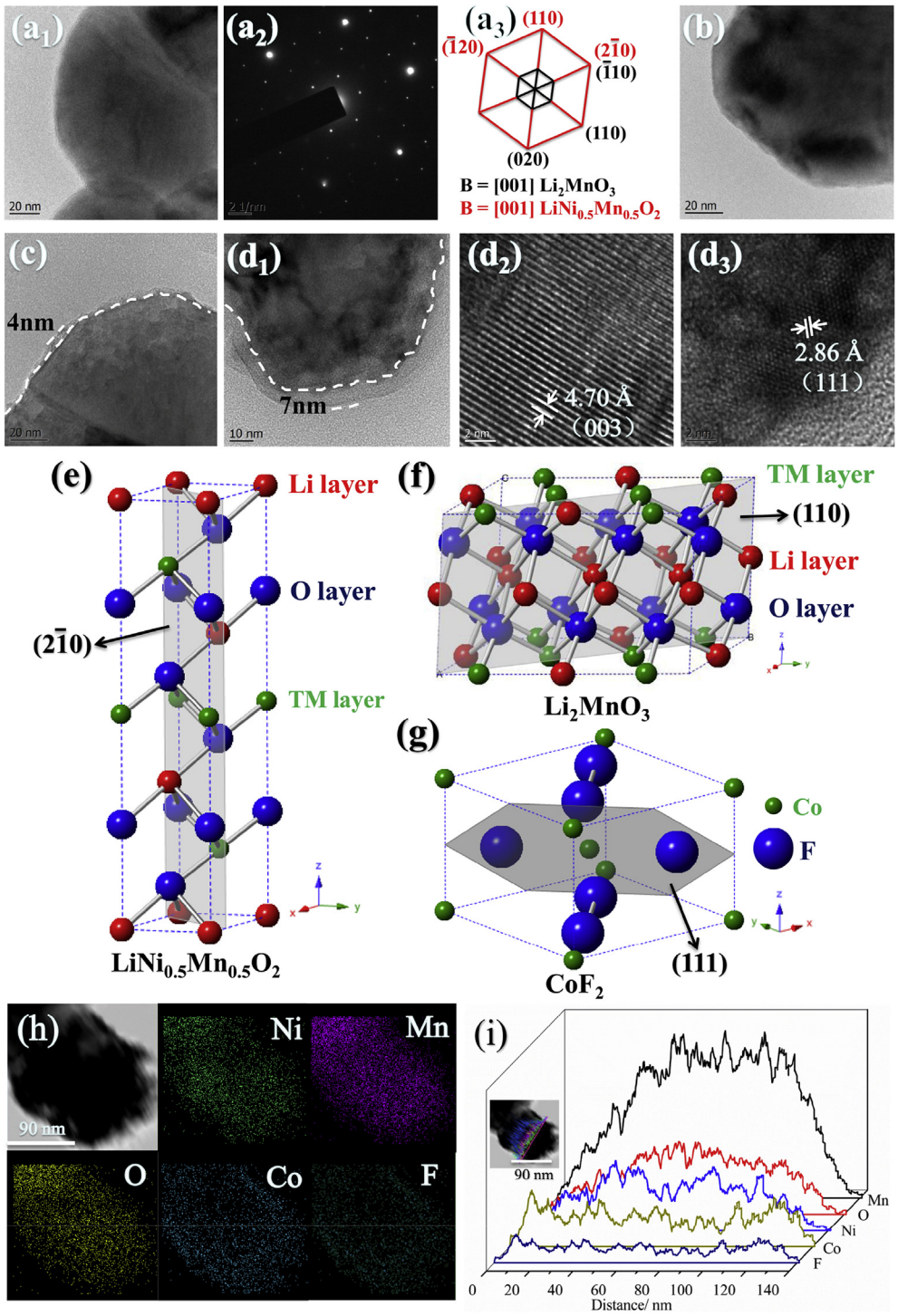

Fig. 3. (a_1) TEM image and (a_2) corresponding SAED pattern of LNMO; TEM images of (b) CF-0.1, (c) CF-0.5 and (d_1) CF-1.0; HRTEM images of (d_2) inner and (d_3) edge region for CF-1.0; The crystal structures of (e) hexagonal $LiNi_{0.5}Mn_{0.5}O_2$, (f) monoclinic Li_2MnO_3 and (g) cubic CoF_2; (h) TEM image and corresponding EDS elemental mapping of CF-1.0; (i) EDS line scan signals of CF-1.0.

3.2. Electrochemical performance

3.2.1. Initial charge and discharge behavior

To evaluate the effect of CoF_2 coating on the initial electrochemical performance of LNMO, the initial charge-discharge curves of LNMO, CF-0.1, CF-0.5 and CF-1.0 measured at 0.1C between 2.0 V and 4.8 V are shown in Fig. 5(a). It can be seen that all the samples exhibit two distinguished voltage regions during the first charge process. The sloping curve below 4.5 V is attributed to the lithium extraction from $LiNi_{0.5}Mn_{0.5}O_2$ with hexagonal layered structure along with the oxidation of $Ni^{2+}/Ni^{3+}/Ni^{4+}$, and the plateau above 4.5 V is ascribed to the lithium extraction as well as the release of O_2 from monoclinic Li_2MO_3 accompanying with the activation of Li_2MO_3, which generates oxygen-ion vacancy and induces lithium-

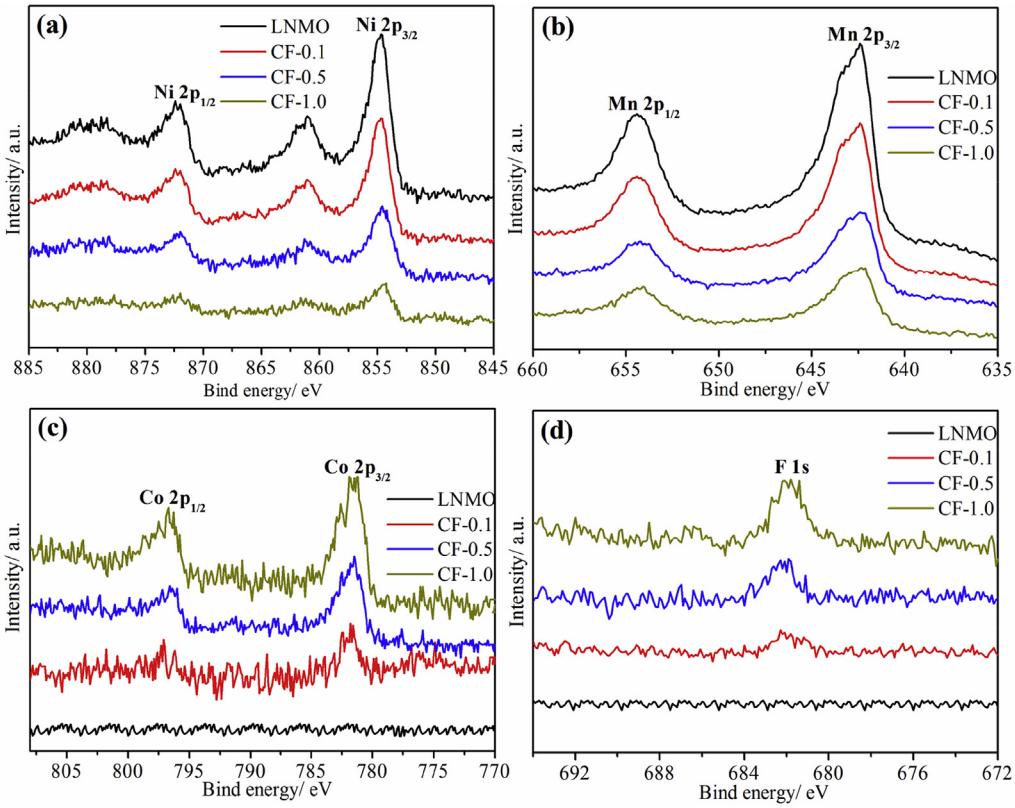

Fig. 4. XPS spectra of LNMO, CF-0.1, CF-0.5 and CF-1.0 in the region of (a) Ni 2p, (b) Mn 2p, (c) Co 2p and (d) F 1s.

ion vacancy in TM layers during initial discharge procedure resulting in a large irreversible capacity loss [31,42,43], corresponding schematic view of extraction/insertion of Li^+ during initial charge-discharge process in LNMO active materials shown in Fig. 5(c). Fig. 5(b) presents the CV profiles of all the samples for the initial cycle. The oxidation peaks of $Ni^{2+}/Ni^{3+}/Ni^{4+}$ at about 3.875–4.0 V as well as the peaks of the release of O_2 at about 4.75 V can be observed clearly for all the samples during initial charge process, while the peak intensity of the release of O_2 weakens gradually as the increase of CoF_2 coating amount in consequence of effective suppression of the loss of O_2 by nano-coating layer. And the reduction peaks of $Ni^{4+}/Ni^{3+}/Ni^{2+}$ at approximately 3.75 V as well as the weak reduction peaks corresponding to Mn^{4+}/Mn^{3+} couple at about 3.25 V during initial discharge process are observed. Besides, the intensity of reduction peaks of Mn^{4+}/Mn^{3+} wanes with increasing the amount of CoF_2 coating as a result of the reduction of MnO_2 with electrochemical activity after the activation of Li_2MnO_3, consistent with the change tendency of the release of O_2.

As shown in Fig. 5(a), all the samples deliver similar initial charge capacity, while CF-0.1, CF-0.5 and CF-1.0 samples exhibit higher initial discharge capacities of 254.3 mAh g^{-1}, 264.4 mAh g^{-1} and 259.1 mAh g^{-1} as well as larger first coulombic efficiencies of 82.1%, 86.2% and 84.4% than bare LNMO (244.0 mAh·g^{-1} and 75.5%), respectively, which mainly attributed to the suppression of side reaction between electrolyte and active material at high potential by CoF_2 protective layer, less electrolyte oxidation resulting from less oxygen removal, proved by CV results (Fig. 5(b)), and additional capacity provided by reduction reaction of CoF_2 during initial discharge process, the electrochemical conversion reactions of CoF_2 shown as follows:

$$CoF_2 + 2Li^+ + 2e^- \rightarrow Co + 2LiF$$ [31].

Especially, the initial discharge capacity and coulombic efficiency of CF-1.0 slightly decrease compared to CF-0.5, which is responsible for the relatively thicker coating layer restraining overmuch the loss of O_2.

3.2.2. Cyclic performance and rate capability

Fig. 6(a) shows the cycling stability of all the cathode materials measured at 0.1C in the voltage range of 2.0–4.8 V. CF-0.1, CF-0.5 and CF-1.0 exhibit the discharge capacity of 207.2 mAh g^{-1}, 225.3 mAh g^{-1} and 241.0 mAh g^{-1} with the capacity retention of 81.5%, 85.2% and 93.0% after 100 cycles, respectively, while much lower discharge capacity of 153.7 mAh g^{-1} and capacity retention of 63.0% for bare LNMO is obtained at 0.1C. The reason for this superior cyclic stability, which generally enhances as the content of CoF_2 nano-coating increases, involves two aspects. One reason can be the subdued interfacial reaction and the reduction of TM dissolution benefiting from the protection of coating layer. The other reason is the reduction of Li^+ irreversible dissolution and TM migration owing to less amount of O_2 release, which suppresses the phase transformation from layer to spinel structure upon cycling.

Voltage decay resulting from the layer-spinel structure conversion, which gives rise to serious decrease in energy density upon cycling, is one of the major issues for Li-rich cathode materials [44,45]. The discharge voltage stability curves of all the samples upon cycling shown in Fig. 6(b), are employed to evaluate the voltage decay. The LNMO cathode material suffers from the serious voltage fading with a large voltage drop of 0.675 V at 0.1C after 100 cycles, while the values of voltage drop for CF-0.1, CF-0.5 and CF-1.0 are 0.542 V, 0.482 V and 0.312 V, respectively. Obviously, the voltage fading rate efficiently slowed down as the increase of CoF_2 coating content, which can be attributed to the weak electrode/electrolyte interfacial reaction and the enhancement of structural

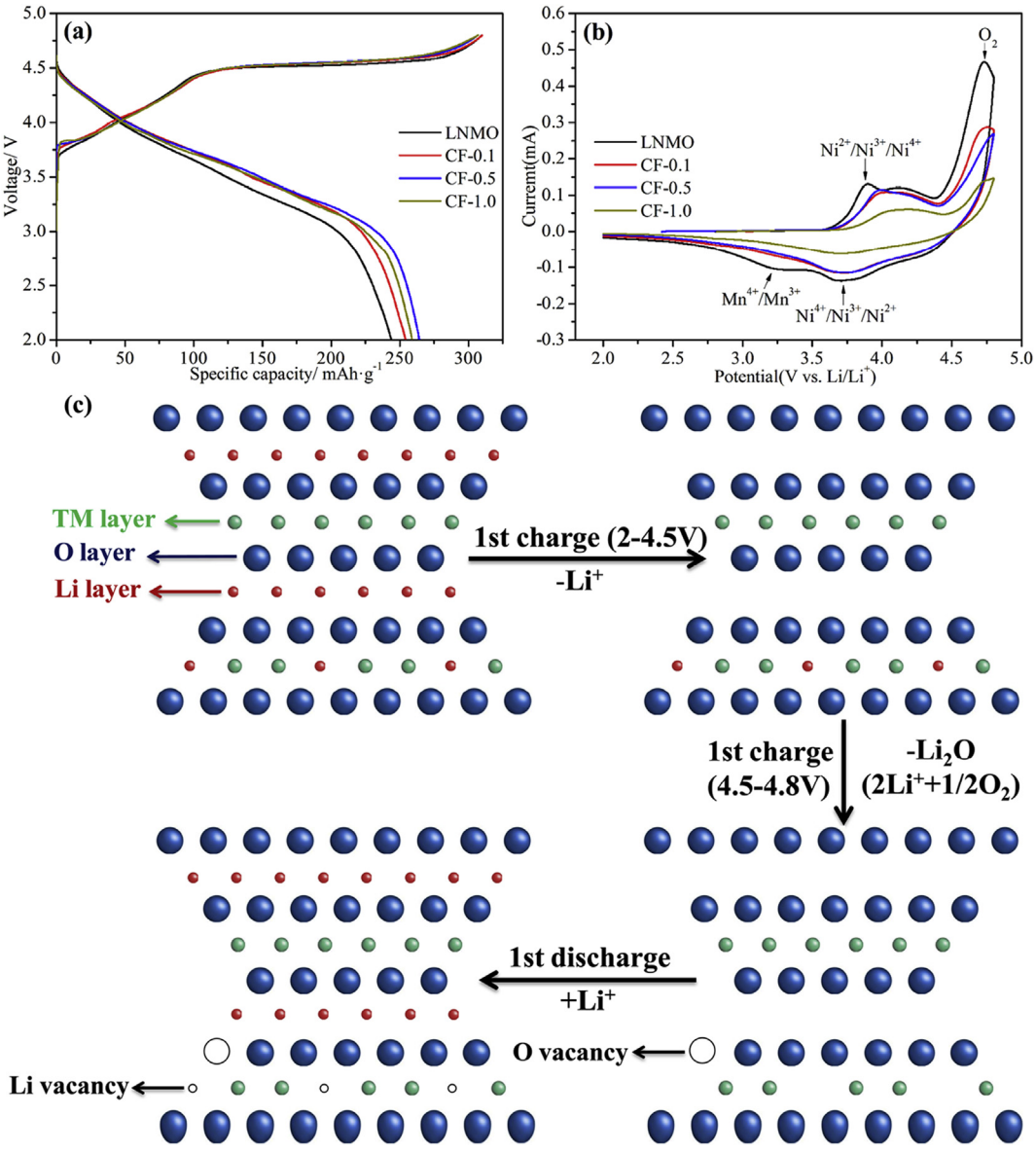

Fig. 5. (a) Initial charge-discharge curves of bare LNMO, CF-0.1, CF-0.5 and CF-1.0 from 2.0 V to 4.8 V at 0.1C and (b) corresponding cyclic voltammetry profiles; (c) schematic view of extraction/insertion of Li^+ during initial charge-discharge process for LNMO active materials.

stability.

Fig. 6(c) presents energy density fading curves upon cycling, which reflect the integration stability of capacity and voltage. CF-0.1, CF-0.5 and CF-1.0 reveal much higher initial energy densities of 914.9 Wh kg^{-1}, 949.1 Wh kg^{-1} and 926.7 Wh kg^{-1}, respectively, compared with 872.9 Wh kg^{-1} for LNMO, as a result of improved initial discharge capacities and similar operating voltage after CoF_2 coating. Accordingly, the excellent stability of capacity and voltage for CF-1.0 delivers the highest retention value of 84.9% after 100 cycles despite reducing on the first discharge capacity than CF-0.5, while LNMO exhibits the lowest retention value of 51.1%.

In order to investigate the capacity and voltage stability for the sample whose CoF_2 coating content is higher than 1.0 wt%, Fig. S1 in supplementary materials presents the operation voltages versus specific capacities of 2.0 wt% CoF_2-coated sample (CF-2.0) and other four samples after 1st cycle and 100^{th} cycle, respectively. The initial discharge capacity of 236.0 mAh g^{-1} and operating potential of 3.444 V for CF-2.0, lower than other four samples, are obtained. On the one hand, the relatively thicker coating layer not only suppresses excessively the release of O_2 but also prevents the extraction/insertion of Li^+ in layered structure, resulting in low capacity. On the other hand, the low reduction potential of 2.854 V for CoF_2/LiF can reduce the operating voltage of CF-2.0. Moreover, CF-2.0 exhibits the improved stability with the capacity retention of 93.6% and the value of voltage drop of 0.299 V after 100 cycles as shown in Fig. S1(inset a and b), which is close to the results of CF-1.0. However, CF-2.0 delivers the much lower energy density of 694.6 Wh kg^{-1} than CF-0.5 and CF-1.0 owing to its low capacity and voltage. Thus, CF-1.0 reaches the optimal integrated performance between high capacity, high operating voltage and outstanding cycling stability.

The excellence in rate capability, performed at various current densities from 0.1 C to 5 C between 2.0 and 4.8 V, further highlights the advantage of the CoF_2 coating, as exhibited in Fig. 6(d). Distinctly, the rate performances enhance gradually as the content of CoF_2 coating increases. Such that even at the current density of

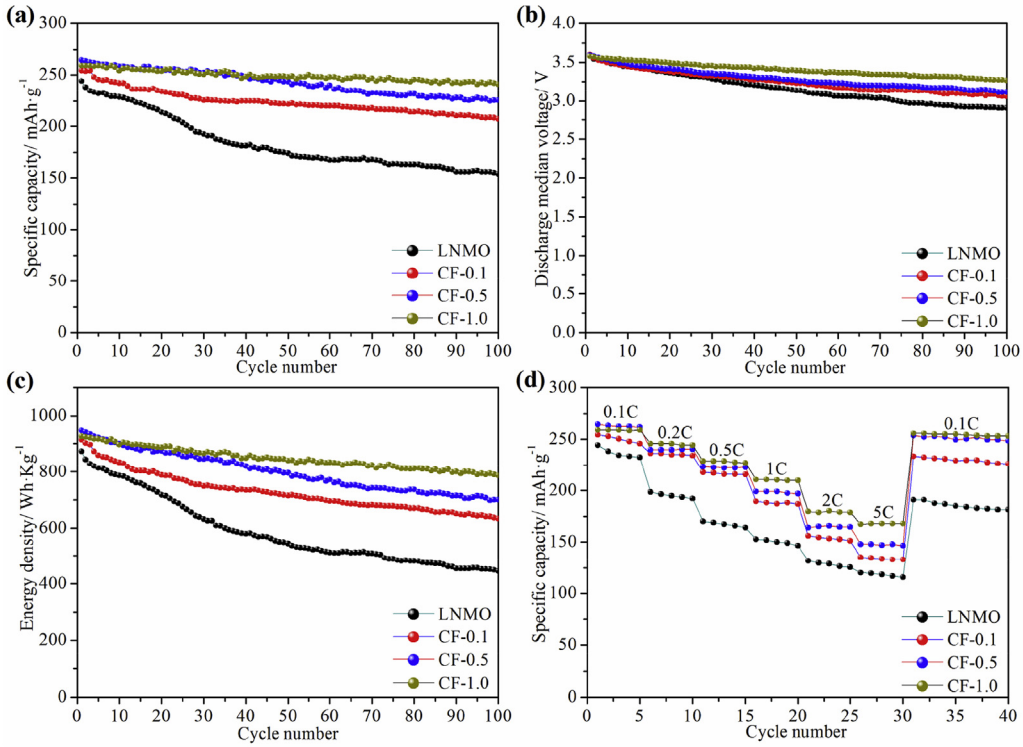

Fig. 6. (a) Cycling performance, (b) discharge median voltage, (c) energy density and (d) rate discharge capability curves of all the samples at 0.1C between 2.0 V and 4.8 V upon cycling.

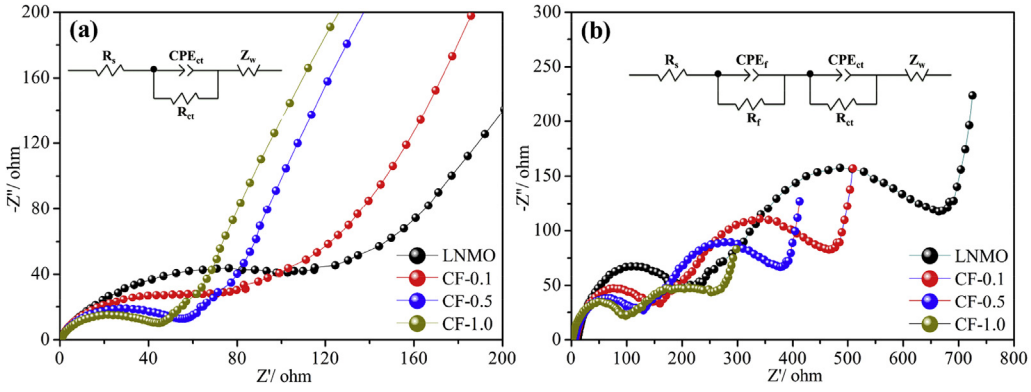

Fig. 7. EIS profiles of LNMO, CF-0.1, CF-0.5 and CF-1.0 (a) at open circuit potential and (b) at charged state of 4.3 V after 100 cycles.

5 C, CF-1.0 exhibits the highest capacity of 167.5 mAh g^{-1}, yet that of LNMO is only 120.1 mAh g^{-1}. Moreover, when the current density is back to 0.1 C, the discharge capacity returns to 98.7% of its initial value for CF-1.0, implying good reversibility and structural stability after high-rate measurements. The primary reason for the significantly improved rate capability of CF-1.0 is that the introduction of CoF_2 nano-coating layer, which accelerates the electrons transport and Li^+ diffusion, and inhibits the interfacial reaction between electrolyte and active materials.

3.3. Improved electrochemical kinetics in CoF_2 nano-coating layer

To get insight into the causes for significantly improved cyclic stability and rate performance of CoF_2-coated samples, EIS measurements of all five samples were performed respectively, whose Nyquist plots are shown in Fig. 7 and the experimental results are fitted with the equivalent circuits in the inset. Fig. 7(a) presents the EIS curves of the cells at open circuit potential before cycling. The intercept on the x-axis at the highest frequency is related to ohmic resistance of the electrolyte (R_s), the diameter of the semicircle represents charge-transfer resistance (R_{ct}), and the slope line at the low frequency is assigned to the Warburg impedance (Z_w) exhibiting the diffusion of Li^+ in the electrode material. It can be obviously seen that a significant decrease in the R_{ct} with the increase of CoF_2 coating amount except for the similar values of R_s and Z_w, exhibiting better electrochemical kinetics on the electrode/electrolyte interface for CF-1.0. The EIS spectra at the charged potential of 4.3 V after 100 cycles at 0.1 C, with a high-frequency semicircle ascribed to the resistance (R_f) of the solid electrolyte interface (SEI) and a medium-frequency corresponding to charge-transfer resistance (R_{ct}), are presented in Fig. 7(b). As expected, CF-1.0 appears the lowest values of R_f and R_{ct}, indicating that the formation and

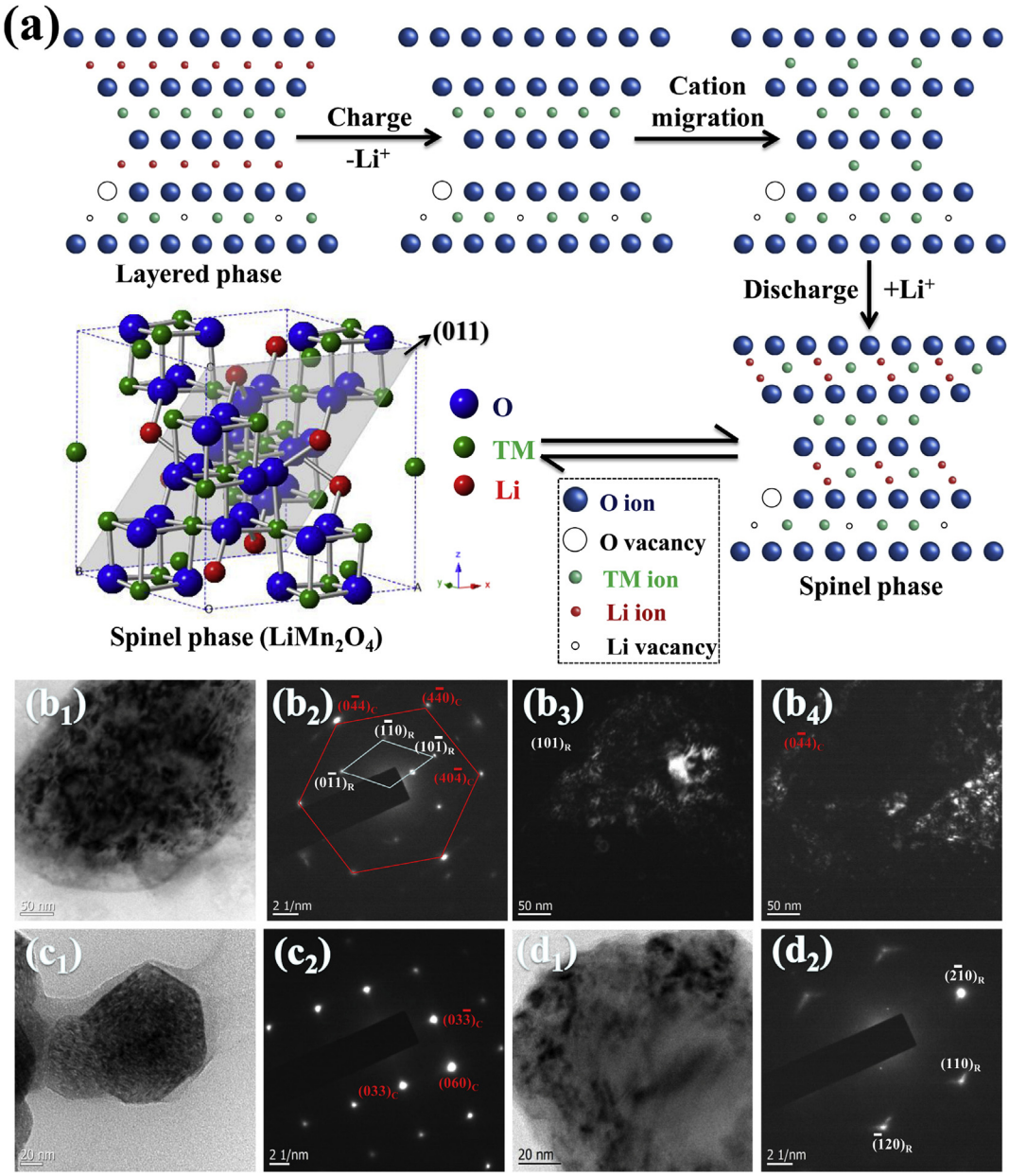

Fig. 8. (a) Schematic view of structural transformation from layered to spinel phase upon cycling for LNMO active materials; (b_1) TEM image, (b_2) corresponding SAED pattern and (b_3 and b_4) dark field images of LNMO after 50 cycles; TEM images and corresponding SAED patterns of: (c_1 and c_2) LNMO after 100cycles, (d_1 and d_2) CF-1.0 after 100 cycles between 2.0 and 4.8 V at 0.1 C. The index marked by subscript R and C is related to the rhombohedral (layered $LiNi_{0.5}Mn_{0.5}O_2$) phase and cubic (spinel $LiMn_2O_4$) phase.

growth of the unacceptable SEI film as well as the interfacial reaction have been mitigated by CoF_2 coating layer. Thus, the improvement of electrochemical kinetics, the suppression of the formation of SEI film and side reaction between electrolyte and electrode, are responsible for the outstanding stability of capacity and rate capability of CF-1.0.

3.4. Delayed phase transition in CoF_2 nano-coating layer upon cycling

To disclose the reasons for improving the capacity fading and voltage decay upon cycling of CoF_2-coated samples, LNMO and CF-1.0 after several cycles were observed using TEM. Fig. 8 (b_1 and b_2) presents TEM image and corresponding SAED pattern of LNMO after 50 cycles at 0.1 C between 2.0 and 4.8 V. Two types of diffraction patterns can be observed, consisting of [111] zone axis of hexagonal layered structure and [111] zone axis of cubic spinel structure. Furthermore, the dark filed images, corresponding to the lattice planes of $(101)_R$ and $(04(__)4)_C$ as shown in Fig. 8(b_3 and b_4), respectively, clearly reveal the structure transformation from layered to spinel phase after 50 cycles and the spinel structure originating from the surface of active material. The phase transition upon cycling is ascribed to the migration of TM ions from TM layers to Li layers induced by the irreversible release of oxygen and extraction of Li^+ after the initial cycle [10,46–48], which leads to serious capacity fading and voltage decay, as illustrated in Fig. 8(a). After 100 cycles for LNMO, a thick layer, namely, SEI film formed on the surface of grain, indicative of the severe side reaction between electrolyte and electrode as shown in Fig. 8(c_1). And the SAED pattern exhibits [100] zone axis of cubic spinel phase on the whole

particle in Fig. 8(c_2), indicating complete structure transition after 100 cycles. However, the thin SEI film mixed with CoF_2 coating layer can be observed in Fig. 8(d_1) for CF-1.0 after 100 cycles owing to the inhibition of the release of oxygen during initial several cycles, meanwhile it still remain in the rhombohedral layered phase, which is in good agreement with the best stability of capacity and operating voltage. Therefore, the phase transition from layered to spinel can be delayed effectively by CoF_2 nano-coating layer upon cycling.

4. Conclusions

In this paper, a nano protective layer of CoF_2, in situ synthesized by means of a common wet chemistry technology, was coated on LNMO. The results of SEM, TEM, EDS and XPS demonstrate that CoF_2 coating, belong to cubic structure, distributes homogeneously on the surface of LNMO, and the cell tests reveal that electrochemical performances are enhanced obviously for CoF_2-coated samples. CF-0.5 delivers the highest initial discharge capacity of 264.4 mAh g^{-1} and coulombic efficiency of 86.2%, benefiting from the electrochemical conversion reaction based on CoF_2/LiF, as well as the reduction in the amount of irreversible O_2 release and the Li^+ vacancies proved by the CV measurements. In addition, the higher first discharge capacity of 259.1 mAh g^{-1} compared to bare LNMO of 244.0 mAh g^{-1}, the excellent cycling stability with the capacity retention rate of 93.0% after 100 cycles at 0.1 C, the improved rate performance with the capacity of 167.5 mAh g^{-1} even at 5 C, and the restraining operating voltage decay with the drop of 0.312 V after 100 cycles at 0.1 C are obtained for CF-1.0 sample. The outstanding electrochemical performances are ascribed to the CoF_2 nano-coating in protection electrode material from deterioration in the electrolyte, the enhancement of kinetics electrochemical involving better electron transfer and Li^+ diffusion, and the inhibition of layered-spinel phase transition initiated from particle edge and spread into inner bulk by means of minimizing the migration of TM ions into Li layers. Therefore, the novel design of CoF_2 nano-coating not only provides a tactic to surmount the defects of LNMO and displays the superior comprehensive effect on improving electrochemical performance among the coatings in published data, but also illuminates in depth the mechanism of capacity fading and voltage decay upon cycling.

Acknowledgement

This work was supported by National Natural Science Foundation of China (Grant no. E51504196), the China Postdoctoral Science Foundation (no. 2012M521760) and the Fundamental Research Funds for the Central Universities (no. xjj2014052).

Appendix A. Supplementary data

Supplementary data related to this article can be found at http://dx.doi.org/10.1016/j.jpowsour.2016.09.028.

References

[1] M.S. Whittingham, Chem. Rev. 104 (2004) 4271–4302.
[2] J.B. Goodenough, Y. Kim, Chem. Mater. 22 (2009) 587–603.
[3] M.M. Thackeray, S.-H. Kang, C.S. Johnson, J.T. Vaughey, R. Benedek, S. Hackney, J. Mater. Chem. 17 (2007) 3112–3125.
[4] X. Bian, Q. Fu, Q. Pang, Y. Gao, Y. Wei, B. Zou, F. Du, G. Chen, ACS Appl. Mater. Interfaces 8 (2016) 3308–3318.
[5] Q.Y. Wang, J. Liu, A.V. Murugan, A. Manthiram, J. Mater. Chem. 19 (2009) 4965–4972.
[6] Z. Wang, E. Liu, L. Guo, C. Shi, C. He, J. Li, N. Zhao, Surf. Coat. Technol. 235 (2013) 570–576.
[7] A.R. Armstrong, M. Holzapfel, P. Novák, C.S. Johnson, S.-H. Kang, M.M. Thackeray, P.G. Bruce, J. Am. Chem. Soc. 128 (2006) 8694–8698.
[8] J. Yan, X. Liu, B. Li, RSC Adv. 4 (2014) 63268–63284.
[9] M. Hou, J. Liu, S. Guo, J. Yang, C. Wang, Y. Xia, Electrochem. Commun. 49 (2014) 83–87.
[10] M. Xu, J. Mater. Chem. A 3 (2015) 13933–13945.
[11] B. Li, J. Mater. Chem. A 3 (2015) 21290–21297.
[12] P.R. Ilango, T. Subburaj, K. Prasanna, Y.N. Jo, C.W. Lee, Mater. Chem. Phys. 158 (2015) 45–51.
[13] F. Wu, Z. Wang, Y. Su, N. Yan, L. Bao, S. Chen, J. Power Sources 247 (2014) 20–25.
[14] S. Shi, J. Tu, Y. Tang, X. Liu, Y. Zhang, X. Wang, C. Gu, Electrochim. Acta 88 (2013) 671–679.
[15] Y. Liu, S. Liu, Y. Wang, L. Chen, X. Chen, J. Power Sources 222 (2013) 455–460.
[16] S. Shi, J. Tu, Y. Zhang, Y. Zhang, X. Zhao, X. Wang, C. Gu, Electrochim. Acta 108 (2013) 441–448.
[17] J. Zheng, J. Li, Z. Zhang, X. Guo, Y. Yang, Solid State Ion. 179 (2008) 1794–1799.
[18] X. Liu, J. Liu, T. Huang, A. Yu, Electrochim. Acta 109 (2013) 52–58.
[19] X. Liu, T. Huang, A. Yu, Electrochim. Acta 163 (2015) 82–92.
[20] J.-H. Kim, M.-S. Park, J.-H. Song, D.-J. Byun, Y.-J. Kim, J.-S. Kim, J. Alloy. Compd. 517 (2012) 20–25.
[21] T. Zhao, L. Li, R. Chen, H. Wu, X. Zhang, S. Chen, M. Xie, F. Wu, J. Lu, K. Amine, Nano Energy 15 (2015) 164–176.
[22] J. Ma, B. Li, L. An, H. Wei, X. Wang, P. Yu, D. Xia, J. Power Sources 277 (2015) 393–402.
[23] H.G. Song, J.Y. Kim, K.T. Kim, Y.J. Park, J. Power Sources 196 (2011) 6847–6855.
[24] J. Lu, Q. Peng, W. Wang, C. Nan, L. Li, Y. Li, J. Am. Chem. Soc. 135 (2013) 1649–1652.
[25] L.-N. Cong, X.-G. Gao, S.-C. Ma, X. Guo, Y.-P. Zeng, L.-H. Tai, R.-S. Wang, H.-M. Xie, L.-Q. Sun, Electrochim. Acta 115 (2014) 399–406.
[26] Q. Fu, F. Du, X. Bian, Y. Wang, X. Yan, Y. Zhang, K. Zhu, G. Chen, C. Wang, Y. Wei, J. Mater. Chem. A 2 (2014) 7555–7562.
[27] X. Pu, C. Yu, Nanoscale 4 (2012) 6743–6747.
[28] Y. Liu, Q. Wang, X. Wang, T. Wang, Y. Gao, M. Su, A. Dou, Ionics 21 (2015) 2725–2733.
[29] X. Liu, Q. Su, C. Zhang, T. Huang, A. Yu, ACS Sustain. Chem. Eng. 4 (2015) 255–263.
[30] Y. Liu, Q. Wang, Y. Lu, B. Yang, M. Su, Y. Gao, A. Dou, J. Alloy. Compd. 638 (2015) 1–6.
[31] J. Cabana, L. Monconduit, D. Larcher, M.R. Palacin, Adv. Mater. 22 (2010) E170–E192.
[32] H. Li, P. Balaya, J. Maier, J. Electrochem. Soc. 151 (2004) A1878–A1885.
[33] X. Fan, Y. Zhu, C. Luo, L. Suo, Y. Lin, T. Gao, K. Xu, C. Wang, ACS Nano 10 (2016) 5567–5577.
[34] J.-S. Kim, C.S. Johnson, J.T. Vaughey, M.M. Thackeray, S.A. Hackney, W. Yoon, C.P. Grey, Chem. Mater. 16 (2004) 1996–2006.
[35] X. Yang, D. Wang, R. Yu, Y. Bai, H. Shu, L. Ge, H. Guo, Q. Wei, L. Liu, X. Wang, J. Mater. Chem. A 2 (2014) 3899–3911.
[36] Y. Li, X.-q. Niu, D.-h. Wang, D. Zhou, X.-l. Wang, C.-d. Gu, J.-p. Tu, J. Mater. Chem. A 3 (2015) 14291–14297.
[37] J. Lin, D. Mu, Y. Jin, B. Wu, Y. Ma, F. Wu, J. Power Sources 230 (2013) 76–80.
[38] L. Xiao, J. Xiao, X. Yu, P. Yan, J. Zheng, M. Engelhard, P. Bhattacharya, C. Wang, X.-Q. Yang, J.-G. Zhang, Nano Energy 16 (2015) 143–151.
[39] M.E. Spahr, P. Novák, B. Schnyder, O. Haas, R. Nesper, J. Electrochem. Soc. 145 (1998) 1113–1121.
[40] C. Wagner, W. Riggs, L. Davis, Physical Electronics Division, Perking Elmer Corporation, 1979, pp. 74–80.
[41] J. Liu, A. Manthiram, J. Mater. Chem. 19 (2010) 3961–3967.
[42] X. He, J. Wang, R. Kloepsch, S. Krueger, H. Jia, H. Liu, B. Vortmann, J. Li, Nano Res. 7 (2014) 110–118.
[43] S. Chong, Y. Liu, W. Yan, Y. Chen, RSC Adv. 6 (2016) 53662–53668.
[44] J.C. Knight, A. Manthiram, J. Mater. Chem. A 3 (2015) 22199–22207.
[45] D. Wang, I. Belharouak, G. Zhou, K. Amine, Adv. Funct. Mater. 23 (2013) 1070–1075.
[46] E.-S. Lee, A. Manthiram, J. Mater. Chem. A 2 (2014) 3932–3939.
[47] B. Xu, C.R. Fell, M. Chi, Y.S. Meng, Energy Environ. Sci. 4 (2011) 2223–2233.
[48] A. Boulineau, L. Simonin, J.-F. Colin, C. Bourbon, S. Patoux, Nano Lett. 13 (2013) 3857–3863.